Materials Transactions, JIM, Vol. 33, No. 8 (1992), pp. 723 to 729

High Mechanical Strength of Quasicrystalline Phase Surrounded by fcc-Al Phase in Rapidly Solidified Al-Mn-Ce Alloys

A. Inoue*, M. Watanabe**, H. M. Kimura*, F. Takahashi**†, A. Nagata** and T. Masumoto*

*Institute for Materials Research, Tohoku University, Sendai 980, Japan
**Department of Materials Engineering and Applied Chemistry, Mining College, Akita University, Akita 010, Japan

A nonequilibrium structure consisting of fine quasicrystalline (icosahedral) grains surrounded by fcc-Al phase was found to form in rapidly solidified Al-Mn-Ce alloys. The formation of the nonequilibrium structure is limited to a composition range of 4 to 6 at% Mn and 2 to 3%Ce which is located around the phase boundary between fcc solid solution and icosahedral plus amorphous phases. The icosahedral phase consists of equiaxed grains with a size of 50 to 100 nm and the width of the fcc-Al phase along the grain boundary is as small as 5 to 15 nm. The mixed phase alloys have good bending ductility and exhibit high tensile fracture strength (σ_f) of 960 to 1320 MPa. It should be noticed that the high σ_f values exceeding 1000 MPa are obtained for the Al-rich alloys containing the quasicrystalline phase. It is thus concluded that the lanthanide (Ce) element has a useful effect on the achievement of high mechanical strengths and good ductility through a significant structural modification resulting from the increase in the quenching effect.

(Received April 21, 1992)

Keywords: *rapid solidification, aluminum-manganese-cerium alloy, surrounding Al phase, coexistent icosahedral and Al phases, high specific strength, good ductility*

I. Introduction

Recently, Al-based amorphous alloys have been produced by liquid quenching methods such as melt spinning[1][2] and high-pressure gas atomization[3]. Furthermore, their amorphous alloys have been reported to exhibit high tensile fracture strengths reaching 1250 MPa in an amorphous single phase state[4] and 1560 MPa in a mixed state consisting of nanoscale fcc-Al particles embedded in an amorphous matrix[5]. However, the amorphous alloy systems in which high tensile fracture strengths exceeding 1000 MPa are obtained are limited to the Al-Ln-Ni (Ln=lanthanide metal) system[6]. The complete replacement of Ni by other transition metals causes the ductile-brittle transition for Ti, V, Cr, Mn, Fe or Co and the decrease in tensile strength for Cu, though the replacement only by Cu keeps a good ductile nature[7]. On the other hand, the mechanical properties of fcc supersaturated solutions in rapidly solidified $Al_{92}M_5Si_3$ (M=transition metal) alloys were examined systematically with the aim of searching an appropriate M element for the achievement of higher mechanical strengths. As a result, Mn has been clarified to cause the highest values of tensile strength and hardness for the fcc solutions without detriment to good ductility[8][9]. The reason for the achievement of the high mechanical strengths for the Al-based alloys containing Mn has been interpreted on the basis of the information[10] that Mn has an appropriate outer electron concentration for the bonding against Al as well as a high formation tendency of a quasicrystalline phase with high resistance against plastic deformation. This interpretation suggests the possibility that the application of rapid solidification to the Al-Mn-Ln system results in a high mechanical strength exceeding the highest strength of the fcc solution in Al-Mn-Si system by an appropriate structure control including the homogeneous dispersion of fine quasicrystalline grains.

More recently, the present authors have performed a search of obtaining high mechanical strengths by taking advantage of the high resistance against plastic deformation for the quasicrystalline phase. As a result, we found that the Al-Mn-Ce alloys containing an icosahedral quasicrystal as a main phase exhibit high tensile fracture strengths exceeding 1000 MPa combined with good ductility even at the Al-rich compositions of 92 and 93 at%. This paper is intended to present the composition range, microstructure and mechanical properties of the rapidly solidified Al-Mn-Ce alloys exhibiting tensile strengths above 1000 MPa.

II. Experimental Procedure

Binary Al-Mn and ternary Al-Mn-Ce alloys were used in the present study. The ingots were prepared by induction-melting a mixture of pure Al (99.99 mass%), Mn (99.99 mass%) and Ce (99.9 mass%) metals in a purified argon atmosphere. The compositions are nominally expressed in atomic per cent. From the master alloy ingots, ribbons with a cross section of about 0.02 mm × 1 mm were prepared by a single roller melt-spinning technique in an argon atmosphere. The as-quenched and annealed

† Graduate Student, Akita University.

structures of the melt-spun ribbons were examined by X-ray diffractometry and transmission electron microscopy (TEM) techniques. Thin foils for TEM were prepared by electrolytic polishing in an electrlyte of perchloric acid and acetic acid with a 1:9 volumetric ratio. TEM observation and microanalysis were performed on a JEOL 2000FX analytical microscope equipped with an energy dispersive X-ray spectrometer (EDXS) with a Model TN-5500 analyzer system for standard-less analysis of the thin films. The decomposition behavior of as-quenched phase was also examined by differential scanning calorimetry (DSC) at a scanning rate of 0.67 K/s. Hardness and tensile strength of the ribbon specimens were measured by a Vickers microhardness tester with a 0.98 N (100 gf) load and an Instron-type tensile testing machine at a strain rate of $4.17 \times 10^{-4}\ s^{-1}$, respectively. Eight to ten symmetrical indentations and five tensile test data were used to determine the average microhardness value and tensile fracture strength. Tensile specimens were cut from the melt-spun ribbon into strips having a gauge dimension of 20 mm long for fracture strength. Subsequent to tensile testing, the cross-sectional area at the fracture site of each specimen was measured by optical microscopy and/or scanning electron microscopy in order to minimize errors in the estimation of the tensile strength.

III. Results and Discussion

Figure 1 shows the compositional dependence of as-quenched structure in the Al-Mn-Ce system, along with the data of bending ductility and the onset temperature of an exothermic reaction (T_x) due to the decomposition of solid solution or amorphous phase. With increasing Mn and Ce contents, the structure changes from an fcc solution to an amorphous phase through mixed states of fcc+quasicrystalline (icosahedral), fcc+amorphous and icosahedral+amorphous phases. A good ductility, which is shown by a 180 degree bending without fracture, is obtained in the fcc solution in the entire composition range, the coexistent fcc+icosahedral phases in the range of 4 to 6%Mn and 0 to 3%Ce and the coexistent fcc+amorphous phases in the range of 1 to 2%Mn and 4 to 5%Ce. T_x of the quenching-induced nonequilibrium phases is in the range of 545 to 630 K for the fcc solution, 515 to 580 K for the coexistent fcc+icosahedral phases and 550 to 570 K for the coexistent fcc+amorphous phases. T_x in the fcc phase field tends to decrease with increasing solute content presumably because the metastability of the fcc supersaturated solution decreases with increasing the degree of the supersaturation. On the other hand, there is a clear tendency for T_x in the coexistent amorphous and fcc or quasicrystalline phase field to increase with increasing Mn and Ce contents because of the increase in the numbers of the attractive bonding among the constituent elements (Al-Mn, Al-Ce and Mn-Ce pairs) which has been thought[11] to be a dominant factor for the thermal stability of amorphous alloys.

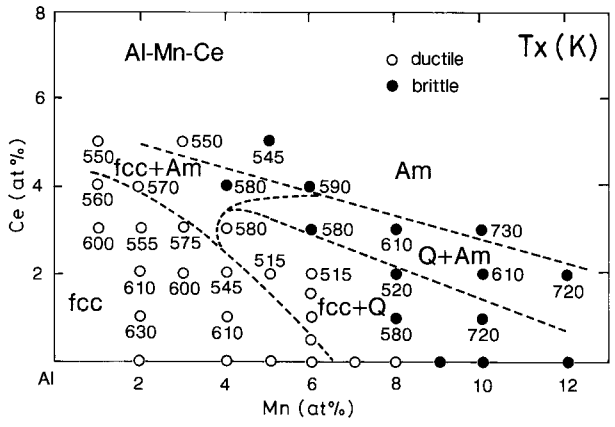

Fig. 1 Compositional dependence of as-quenched phases and decomposition or crystallization temperature (T_x) for rapidly solidified Al-Mn-Ce alloys.

Figure 2 shows the X-ray diffraction patterns taken from the rapidly solidified $Al_{92}Mn_6Ce_2$ and $Al_{91}Mn_7Ce_2$ alloys, along with the data of a rapidly solidified $Al_{92}Mn_8$ alloy. The identification of the icosahedral phase was made using the Elser's indices[12]. The X-ray diffraction peaks except those of fcc-Al phase agree with those of the icosahedral quasicrystal in the Al-Mn alloy and hence the quasicrystalline phase also exists in these Al-Mn-Ce alloys. The diffraction peaks corresponding to the icosahedral phase in the $Al_{92}Mn_6Ce_2$ alloy are rather broad, suggesting that the icosahedral phase consists of very fine grain structure. In order to clarify the

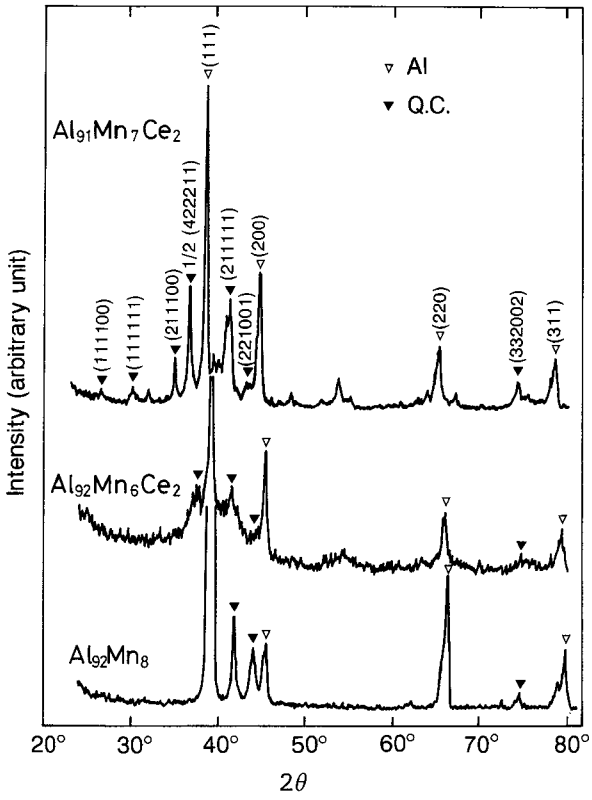

Fig. 2 X-ray diffraction patterns of rapidly solidified $Al_{92}Mn_8$, $Al_{92}Mn_6Ce_2$ and $Al_{91}Mn_7Ce_2$ alloys.

microstructure of the coexistent Al+icosahedral phases with good bending ductility, TEM observation was made for rapidly solidified $Al_{93}Mn_4Ce_3$ and $Al_{92}Mn_6Ce_2$ alloys. As shown in Fig. 3, the as-quenched structure of both the alloys consists of equiaxed icosahedral grains of 50 to 100 nm surrounded by an fcc-Al phase with a width of 5 to 15 nm. As identified in Fig. 3(b) and (d) which are selected area diffraction patterns taken from the circular regions with a diameter of 300 nm, the distinct reflection rings correspond to the icosahedral structure, indicating that the icosahedral equiaxed grains have a random orientation combined with the small grain size. On the other hand, the Al matrix has a fixed crystal orientation on the scale of 300 nm, in spite of the coexistent state with the icosahedral phase.

The confirmation of the unique coexistent structure consisting of equiaxed icosahedral grains and fcc-Al boundary phase was also made by dark-field electron microscopy. Figure 4 shows the bright- and dark-field images of the rapidly solidified $Al_{92}Mn_6Ce_2$ alloy. The dark-field image was taken from the reflection rings of $(211111)_i$ and $(221001)_i$. It is clearly seen that only the equiaxed grains show the bright contrast corresponding to the icosahedral reflection rings and no bright-contrast in the grain boundary phase is seen. The equiaxed grains are concluded to be composed of the icosahedral structure. Similarly, Fig. 5 shows the bright-field image and the dark-field image taken from the reflection spot of $(111)_{Al}$ for the rapidly solidified $Al_{92}Mn_6Ce_2$ alloy. The bright contrast is seen mainly in the grain boundary phase, indicating that the grain boundary phase consists of an fcc-Al structure. In addition to the bright contrast in the grain boundary phase, one can see the bright contrast even in the equiaxed icosahedral grains. The reason for the simultaneous appearance of the bright contrast in the two phases is due to the result that the distance of the $(111)_{Al}$ reflection spot from the (000) spot is nearly the same as that for the $(211111)_i$ and $(221001)_i$ rings and the separation between the fcc-Al and icosahedral spots by the use of an objective aperture is very difficult. Furthermore, the quasicrystalliniety of the equiaxed grains is also confirmed by high-resolution electron microscopy. As shown in Fig. 6, distinct fringe contrast revealing the existence of the long-range periodic lattice is observed only in the grain boundary phase. That is, one cannot see distinct fringe contrast corresponding to the conventional crystalliniety in the equiaxed grains. In addition, as seen in the regions marked with arrows, the phase boundary between the icosahedral and Al phases is smooth and the fringe contrast resulting from the Al phase disappears gradually with the transition from the Al to the icosahedral phase. The gradual disappearance of the fringe contrast suggests that the interface between both the phases is in an appropriate bonding state which

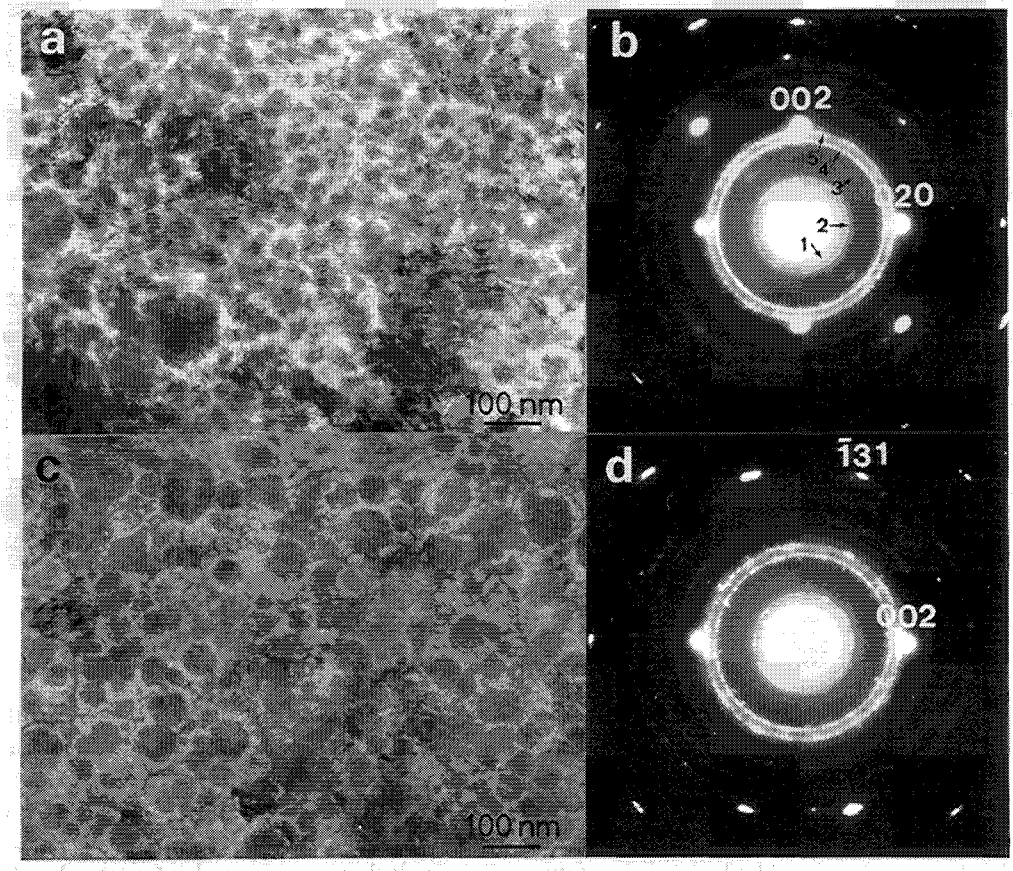

Fig. 3 Bright-field electron micrographs and selected area diffraction patterns of rapidly solidified $Al_{93}Mn_4Ce_3$ (a and b) and $Al_{92}Mn_6Ce_2$ (c and d) alloys. The reflection rings of 1, 2, 3, 4 and 5 in the diffraction pattern (b) are (111000), (111100), (211100), (211111) and (221001) of the icosahedral phase, respectively. The reflection spots indexed in (b) and (d) result from an Al phase and the patterns are identified to be $(100)_{Al}$ and $(310)_{Al}$, respectively.

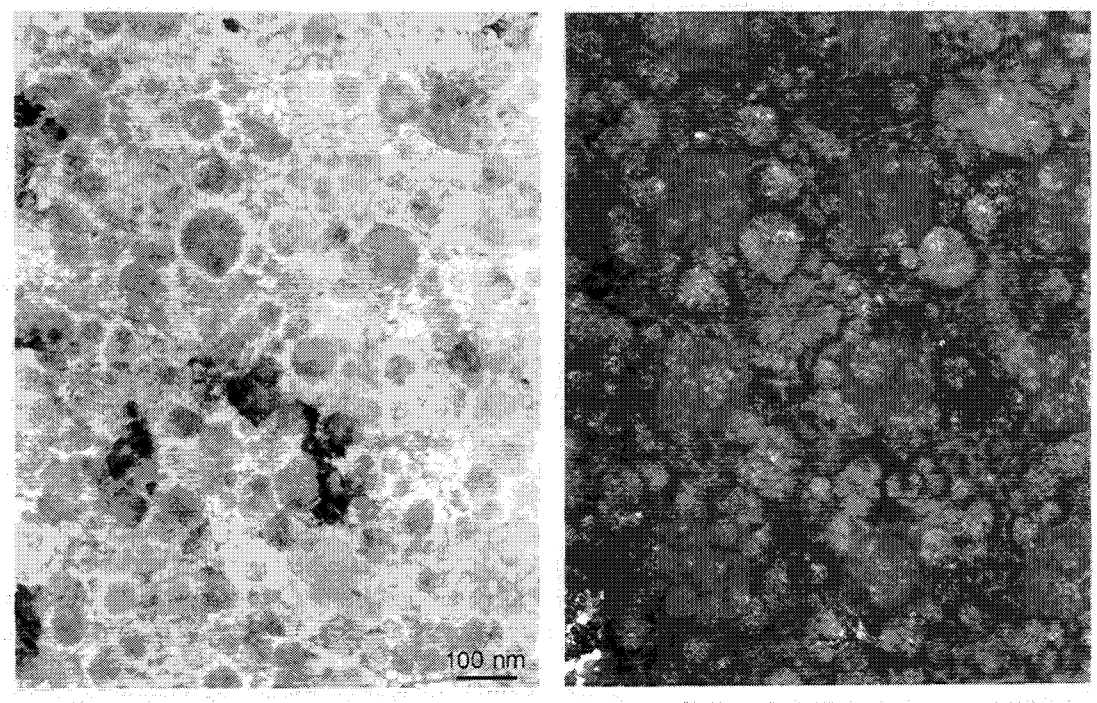

Fig. 4 Bright- and dark-field electron micrographs of a rapidly solidified $Al_{92}Mn_6Ce_2$ alloy. The dark-field image was taken from the $(211111)_i$ and $(221001)_i$ reflection rings of the icosahedral phase.

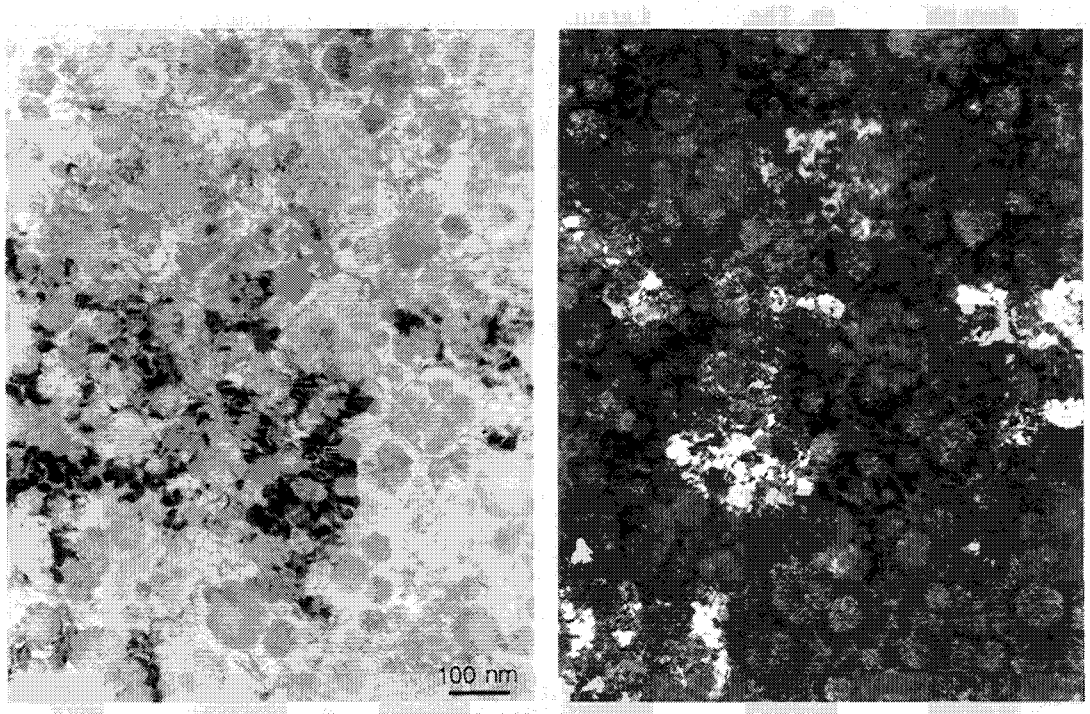

Fig. 5 Bright- and dark-field electron micrographs of a rapidly solidified $Al_{92}Mn_6Ce_2$ alloy. The dark-field image was taken from the $(111)_{Al}$ reflection spot of the fcc-Al which was superimposed on the $(211111)_i$ and $(221001)_i$ reflection rings.

is favorable for the response to applied stress. It should be thus noticed that individual icosahedral grains are surrounded with the thin Al phase and are in an isolated state.

The solute concentrations in the transgranular icosahedral and intergranular fcc-Al phase were examined by the EDXS method, in order to determine an approximate concentration of the icosahedral phase in the Al–Mn–Ce alloy. Table 1 summarizes the Al, Mn and Ce compositions of the transgranular icosahedral and the intergranular fcc-Al phases obtained by the EDXS method from a limited region smaller than about 50 nm in the rapidly solidified $Al_{92}Mn_6Ce_2$ alloy. Additionally, typical examples of the EDXS spectrum taken from the icosahedral spherulite and intergranular Al phase in the Al–Mn–Ce alloy are presented in Fig. 7(a) and (b). As seen in Table 1 and Fig. 7, the average Mn and Ce concentrations in the icosahedral phase are about 7.94 at% and

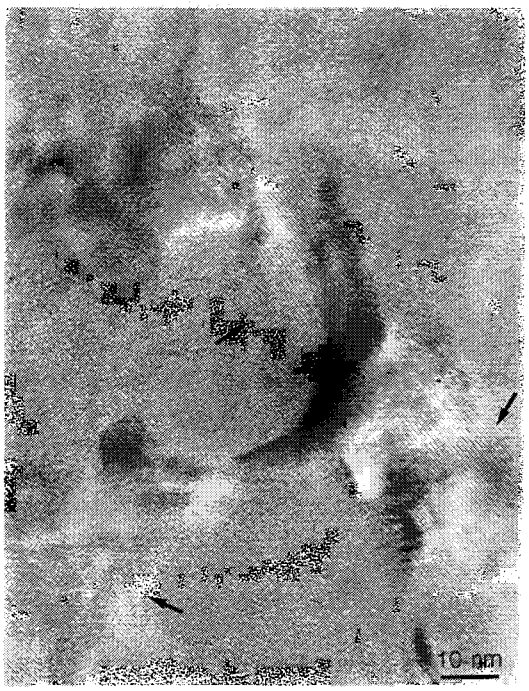

Fig. 6 High-resolution electron micrograph of a rapidly solidified $Al_{92}Mn_6Ce_2$ alloy.

2.54 at%, respectively, and those in the intergranular Al phase are about 4.36 at% and 1.22 at%, respectively. In comparison with the nominal composition ($Al_{92}Mn_6Ce_2$), the Mn and Ce concentrations are higher for the icosahedral phase and lower for the Al phase. However, the solute concentrations of the icosahedral phase are considerably lower than those (18.2 to 22.6 at%Mn)[13] obtained by the same EDXS method for the stoichiometric icosahedral phase in rapidly solidified $Al_{85.7}Mn_{14.3}$ and $Al_{77.5}Mn_{22.5}$ alloys. The significant difference indicates a possibility that the stoichiometric solute concentration of the icosahedral phase shifts to the lower solute concentration side by the dissolution of Ce. However, there is a possibility that the analytical value of the icosahedral phase was obtained from a mixed structure of the icosahedral plus fcc-Al phases because of the difficulty in obtaining the information only from an isolated grain resulting from the fine icosahedral grain sizes. Further detailed analysis with a field-emission type TEM will shed some light on the determination of an exact composition of the stoichiometric icosahedral phase in Al-Mn-Ce ternary system. Based on the above-described experimental data, such a unique coexistent structure is presumed to be formed through the processes of the precipitation of the primary icosahedral phase and the subsequent solidification of the Al phase from the remaining liquidus phase. The reason why the remaining liquid solidifies as an Al phase is presumably because of the enrichment of the solute elements in the primary icosahedral phase. Here, it should be noticed that the mixed phase alloys have a good bending ductility, in spite of the coexistence of the icosahedral phase as a main phase. The good ductility is also thought to result from the extremely small size of the equiaxed quasicrystalline grains as well as good ductility of the film-like fcc phase which surrounds the icosahedral phase.

Table 1 Energy dispersive X-ray microanalytical concentration of transgranular icosahedral and intergranular Al phase in a rapidly solidified $Al_{92}Mn_6Ce_2$ alloy.

Nominal Composition of Alloy (at%)	Analytical Site	Analytical Mn Concentration (at%)	Analytical Ce Concentration (at%)
$Al_{92}Mn_6Ce_2$	transgranular	7.94	4.36
	intergranular	2.54	1.22

It has previously been reported[14][15] that the rapidly solidified $Al_{92}Mn_8$ alloy consists of fcc-Al and icosahedral phases and the icosahedral phase has a dendritic morphology characterized by petaline shape with five-fold symmetry. In addition, the size of the icosahedral phase is of the order of 0.5 μm. In comparison with the previous data on the icosahedral phase in the Al-Mn binary alloy, it is concluded that the icosahedral phase in the Al-Mn-Ce alloys has a more massive (spherical) morphology and a much smaller grain size. Thus, the addition of a small amount of Ce is very effective for the refinement of the icosahedral grains, accompanied by the spheroidization of the shape through the suppression of the anisotropy of grain growth for the icosahedral phase. Here, it appears important to point out that the Ce element leading to the significant modification of the coexistent icosahedral and fcc-Al structure is also effective for the formation of an amorphous phase which can be regarded as an eventual structural modification of the coexistent crystalline structure[16]. The significant structural modification is

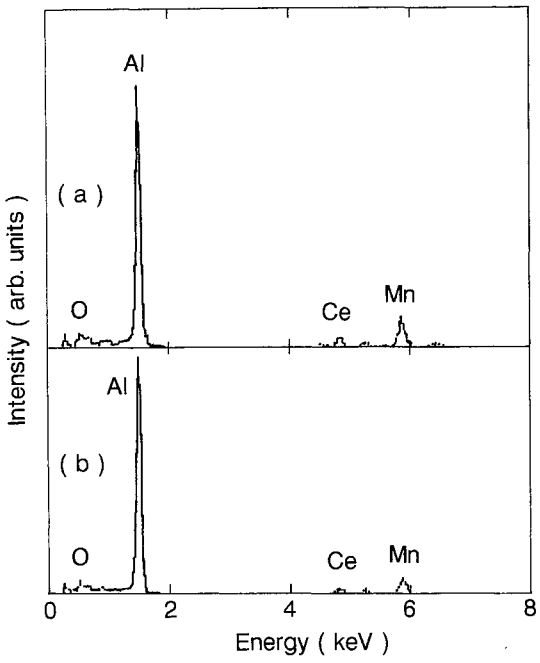

Fig. 7 Energy dispersive X-ray spectra of a rapidly solidified $Al_{92}Mn_6Ce_2$ alloy. (a) Transgranular icosahedral phase, and (b) intergranular Al phase.

presumably due to the suppression of atomic diffusivity through the formation of Al-Ce and Mn-Ce pairs with a stronger bonding nature as compared with that for Al-Mn pair. It is to be expected therefore that a similar structural modification is also achieved by the addition of other lanthanide elements.

Figure 8 shows the compositional dependence of tensile fracture strength (σ_f) for the coexistent Al+icosahedral phases and the fcc-Al solution with good ductility. The σ_f is in the range from 220 to 780 MPa for the fcc-Al solution and from 960 to 1320 MPa for the Al+icosahedral phases. Thus, there is a clear tendency for σ_f to increase with increasing Mn and Ce contents and by the structural change from the fcc to the coexistent Al+icosahedral state. Although the highest σ_f value (780 MPa) for the fcc-Al solution is nearly the same as that (860 MPa)[17] for a supersaturated fcc-Al solution in the Al-Fe-Ce system, the highest σ_f value of the coexistent Al+icosahedral phases is much higher than that for the fcc-Al solution and comparable to that (1250 MPa)[6] for an amorphous phase in Al-Y-Ni-Co quaternary system. This is believed to be the first evidence for the achievement of σ_f exceeding 1000 MPa at the Al-rich compositions of 92 and 93 at% and in the Al-based alloys containing the quasicrystalline phase as a main phase.

Figure 9 shows the scanning electron micrograph revealing the tensile fracture surface of the $Al_{93}Mn_5Ce_2$ alloy having the coexistent Al+icosahedral phases. The fracture occurs along the shear plane which is declined by 45 to 50 degrees to the tensile stress direction. The fracture surface consists of a smooth region caused by the shear sliding and a vein region caused by final rupture after the shear sliding. The rather large area fraction of the smooth region indicates that the mixed phase alloy has a good ductility. Furthermore, the distinct ledge pattern is presumed to be formed through the adiabatic final fracture of the Al phase which lies along the grain boundary of the icosahedral phase.

Vickers hardness also shows a similar compositional dependence for the fcc-Al solution and the coexistent Al+icosahedral and Al+amorphous phases with good bending ductility, as shown in Fig. 10. H_v is in the range of 205 to 400 for the fcc-Al solution, 300 to 460 for the Al+icosahedral phases and 275 to 325 for the Al+amorphous phases, being considerably higher for the coexistent Al+icosahedral structure. Furthermore, there is a clear tendency for H_v to increase with increasing Mn and Ce contents.

IV. Discussion

It is shown in section III that the rapidly solidified structure in the Al-Mn-Ce alloys ranging from 4 to 6%Mn and 3 to 4%Ce consists of fine icosahedral grains surrounded by fcc-Al phase. When the equiaxed grain is assumed to be composed only of an icosahedral phase, the approximate volume fraction of the icosahedral and Al phases is evaluated to be 84 and 16%, respectively. As described above, the nonequilibrium icosahedral single phase in rapidly solidified Al-Mn binary alloys has been reported[13][18] to form in the range 20 to 22 at%Mn. Although the dissolution of Ce element is expected to cause the decrease of the Mn content in the icosahedral single phase, the volume fraction ($\cong$84%) of the icosahedral phase in the range of 4 to 6%Mn and 3 to 4%Ce seems to be overestimated. In addition, judging from the previous result that all the icosahedral alloys are in an extremely brittle state at room temperature, it is not easy to clarify the reason for the good ductility for the Al-Mn-Ce alloys containing icosahedral phase of about 84% in volume per cent. Accordingly, there is a possibility that the equiaxed icosahedral grains with a small size of 50 to 100 nm are composed of either the nanoscale mix-

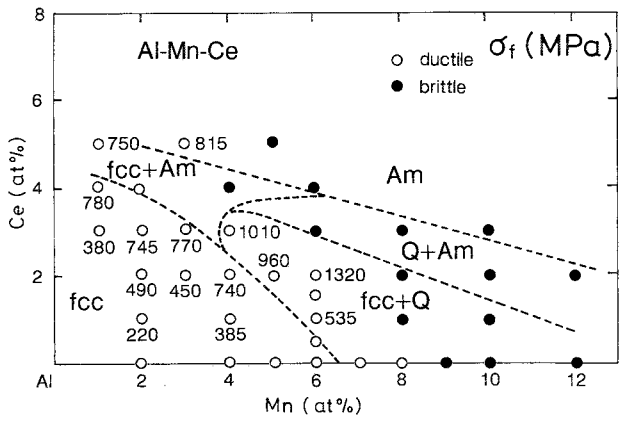

Fig. 8 Compositional dependence of tensile fracture strength (σ_f) for rapidly solidified Al-Mn-Ce alloys.

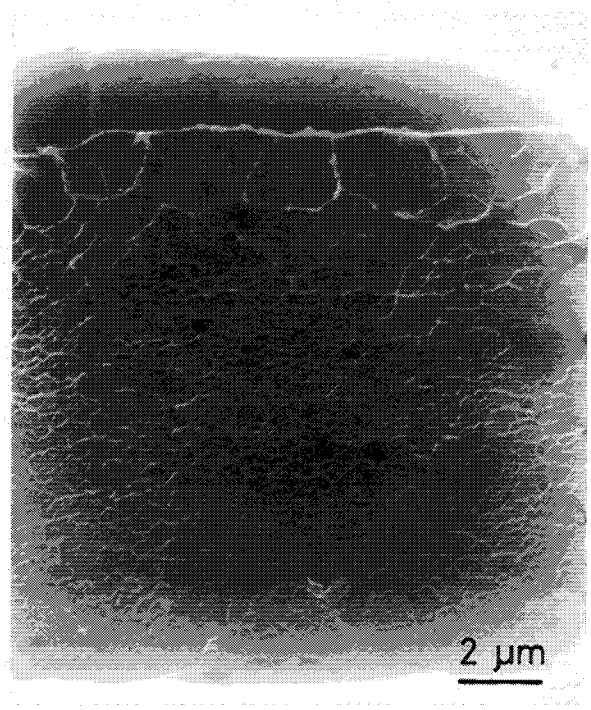

Fig. 9 Scanning electron micrograph revealing the tensile fracture surface of a rapidly solidified $Al_{92}Mn_6Ce_2$ alloy.

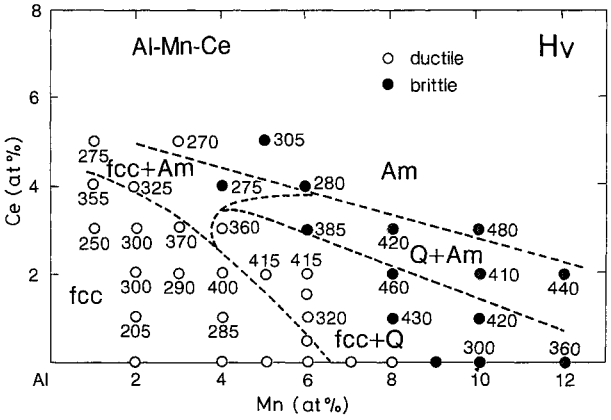

Fig. 10 Compositional dependence of Vickers hardness (H_v) for rapidly solidified Al-Mn-Ce alloys.

ture of icosahedral and Al phases or a unique icosahedral single phase which can be formed even at the small solute concentrations. As shown in Fig. 6, we do not have any evidence for the coexistence of the two phases even by high-resolution electron microscopy. Accordingly, it may be presumed that the equiaxed grains are composed of a unique icosahedral phase with small solute concentrations and the low solute content in the icosahedral phase gives rise to the achievement of the good ductility. The formation of the icosahedral phase at low solute concentrations is interpreted to be obtained by the remarkable extension of the icosahedral phase field to the lower solute concentration side through the increased quenching effect for the Ce-containing Al-Mn alloys. The increase in quenching effect by the dissolution of Ce into Al-Mn alloys is evident from the result (Fig. 1) that an amorphous phase is formed in the Al-13%Mn alloys containing 2 at% Ce. A similar high-strength alloy combined with good bending ductility is expected to be obtained even in the structure state containing an icosahedral phase through an appropriate alloy design so as to enhance the quenching effect.

V. Conclusion

The coexistent Al + quasicrystalline (icosahedral) structure in which the Al phase lies along the grain boundaries of the icosahedral phase was found to form in rapidly solidified $Al_{93}Mn_4Ce_3$, $Al_{93}Mn_5Ce_2$ and $Al_{92}Mn_6Ce_2$ alloys. These alloy compositions are located around the phase boundary between the Al phase field and the icosahedral plus amorphous phase field. The icosahedral phase in the coexistent structure has grain sizes of 50 to 100 nm and the width of the Al phase along the grain boundary is as small as 5 to 15 nm. The mixed phase alloys exhibit high tensile strength (σ_f) exceeding 1000 MPa and the highest σ_f value reaches as high as 1320 MPa for $Al_{92}Mn_6Ce_2$. It should be noticed that the high σ_f above 1000 MPa is obtained at the Al-rich compositions of 92 to 93 at% and in the alloys containing the icosahedral phase as a main phase. The information that the structural control into the unique mixed phases causes the high σ_f values even at the Al-rich compositions and in the coexistent state with the quasicrystal is very important for the future developments of ultra-high strength materials with light weight.

Acknowledgment

One of the authors (A. Inoue) wishes to thank support for this research by a grant from the Light Metal Educational Foundation, Inc.

REFERENCES

(1) A. Inoue, K. Ohtera, A. P. Tsai and T. Masumoto: Jpn. J. Appl. Phys., **27** (1988), L280.
(2) Y. He, S. J. Poon and G. J. Shiflet: Science, **241** (1988), 1640.
(3) A. Inoue, K. Kita, K. Ohtera, H. M. Kimura and T. Masumoto: J. Mater. Sci. Lett., **7** (1988), 1287.
(4) A. Inoue, N. Matsumoto and T. Masumoto: Mater. Trans., JIM, **31** (1990), 493.
(5) Y. H. Kim, A. Inoue and T. Masumoto: Mater. Trans., JIM, **31** (1990), 747.
(6) A. Inoue, N. Matsumoto and T. Masumoto: Mater. Trans., JIM, **31** (1990), 493.
(7) A. Inoue, K. Ohtera and T. Masumoto: Jpn. J. Appl. Phys., **27** (1988), L1796.
(8) A. Inoue and T. Masumoto: J. Japan Inst. Light Metals, **40** (1990), 453.
(9) A. Inoue, M. Watanabe, H. M. Kimura and T. Masumoto: Sci. Rep. Res. Inst. Tohoku Univ., **A-36** (1991), 59.
(10) T. Masumoto and A. Inoue: Bulletin Japan Inst. Metals, **25** (1986), 99.
(11) H. S. Chen: Rep. Prog. Phys., **43** (1980), 353.
(12) V. Elser: Phys. Rev. B, **32** (1985), 4892.
(13) A. Inoue, L. Arnberg, B. Lehtinen, M. Oguchi and T. Masumoto: Met. Trans., **17A** (1986), 1657.
(14) D. Shechtman and I. A. Blech: Met. Trans., **16A** (1985), 1005.
(15) K. Hiraga, M. Hirabayashi, A. Inoue and T. Masumoto: Sci. Rep. Res. Inst. Tohoku Univ., **32** (1985), 309.
(16) A. Inoue, K. Ohtera, K. Kita and T. Masumoto: Jpn. J. Applied Phys., **27** (1988), L1796.
(17) A. Inoue, H. Yamaguchi, M. Kikuchi and T. Masumoto: Sci. Rep. Res. Inst. Tohoku Univ., **35** (1990), 101.
(18) K. Kimura, T. Hashimoto, K. Suzuki, K. Nagayama, H. Ino and S. Takeuchi: J. Phys. Soc. Japan, **54** (1985), 3217.